Meccanica
DOI 10.1007/s11012-013-9727-6

# A generalized velocity field for plane strain backward extrusion through punches of any shape

**H. Haghighat · P. Amjadian**

Received: 17 September 2012 / Accepted: 15 March 2013


**Abstract** In this paper, the process of plane strain backward extrusion process through arbitrarily curved punches, by means of the upper bound method and the finite element method is investigated. A generalized velocity field is developed and by calculating of the internal, shear and frictional powers, the extrusion force is estimated. Then, by using the developed analytical model, optimum punch lengths which minimize the required extrusion forces, are determined for a wedge shaped punch and a streamlined punch shape. The corresponding results for those two punch shapes are also determined by using a finite element code and compared with the upper bound results. This comparison shows that the upper bound predictions are in good agreement with the FE results.

**Keywords** Backward extrusion · Plane strain · Upper bound · FEM

## 1 Introduction

In backward extrusion, there is no relative movement between the initial billet and the container and this process is characterized by the absence of friction between the initial billet surface and the container. In this process, such as other metal forming processes, calculation and optimization of extrusion force are important. Among various methods of solution, the upper bound technique as an analytical method and the finite element method have been widely used for the analysis of the extrusion process. Even though the finite element gives detailed information, it takes considerable CPU time. Using the upper-bound technique has the merits of saving computer's CPU and it appears to be a useful tool for analyzing metal forming problems when the objective of such an analysis is limited to prediction of deformation load and/or to study metal flow during the process.

A number of people have used the upper bound method to analyze the extrusion process through a variety of die shapes. Avitzur [1–4] developed models for axisymmetric extrusion through conical dies using the upper bound approach. Hillier and Johnson [5] used slip line field method to analysis of plane strain forward extrusion through curved dies. Avitzur [6] examined plane strain extrusion through a wedge shaped die using upper bound method. D'Alia [7] proposed approximate formulas for drawing and extruding processes. Chen and Ling [8] developed a velocity field for axisymmetric extrusions through cosine, elliptic and hyperbolic dies. Zimmerman and Avitzur [9] also modeled extrusion using the upper bound method with generalized shear boundaries. Yang et al. [10] as well as Yang and Han [11] developed upper bound models with streamlined dies. Chen and Ling [12] and Nagpal [13] were among the investigators who

H. Haghighat (✉) · P. Amjadian
Mechanical Engineering Department, Razi University, Kermanshah, Iran
e-mail: hhaghighat@razi.ac.ir

Published online: 26 March 2013

explored alternative die shapes, developing velocity fields for axisymmetric extrusions through arbitrarily shaped dies. Chen et al. [14] and Liu and Chung [15] used finite element analysis to examine axisymmetric extrusion through conical dies. Kim et al. [16] used FEM to design an axisymmetric controlled strain rate die. Weinberger [17] derived conditions which must be satisfied by the steady flow of a rigid-plastic material through an extrusion die which minimizes dissipation power. Bakhshi et al. proposed an optimum punch profile in axisymmetric backward rod extrusion [18]. Saboori et al. studied the energy consumption in axisymmetric forward and backward rod extrusion [19]. Gordon et al. developed the adaptable die design method for axisymmetric extrusion and described it in details in a series of papers [20–22]. Haghighat and Amjadian proposed two kinematically admissible velocity fields based on assuming proportional angles and proportional distances from the midline in the deformation zone in upper bound models for plane strain forward extrusion through arbitrarily curved dies [23].

The purpose of this paper is to develop a velocity field that is applicable to plane strain backward extrusion through arbitrarily curved punches. The proposed velocity field is used to find out an optimal wedge shaped die and a streamlined die shape and the corresponding extrusion forces for a given process conditions. The investigation is also performed using the finite element software, ABAQUS.

## 2 Upper bound analysis

Based on the upper bound theory, for a rigid-plastic Von-Misses material and amongst all the kinematically admissible velocity fields, the actual one that minimizes the power required for material deformation is expressed as

$$J^* = \frac{2}{\sqrt{3}}\sigma_0 \int_v \sqrt{\frac{1}{2}\dot{\varepsilon}_{ij}\dot{\varepsilon}_{ij}}\,dv + \frac{\sigma_0}{\sqrt{3}}\int_{S_v} |\Delta V|\,dS + m\frac{\sigma_0}{\sqrt{3}}\int_{S_f} |\Delta V|\,dS - \int_{S_t} T_i V_i\,dS \tag{1}$$

where $\sigma_0$ is the mean flow stress of the material, $\dot{\varepsilon}_{ij}$ the strain rate tensor, $m$ the constant friction factor, $v$ the volume of plastic deformation zone, $S_v$ and $S_f$ the area of velocity discontinuity and frictional surfaces respectively, $S_t$ the area where the tractions may occur, $\Delta V$ the amount of velocity discontinuity on the frictional and discontinuity surfaces and $V_i$ and $T_i$ are the velocity and tractions applied on $S_t$, respectively.

Figure 1 shows two types of the plane strain extrusion process, type I and type II, and their parameters in a schematic diagram. Taking into account the symmetry of the problem, only half of the sections are considered. The material starts as a strip of thickness $2t_o$ and is extruded into a strip product of thickness $2t_f$ through an arbitrarily curved punch in extrusion process type I and a U shape product in process type II. To analyze the process by using the upper bound method, the material under deformation is divided into three zones, as shown in Figs. 1a–1b. In zone I, material is stationary and in zone III the material moves rigidly with the velocity $V_f$. Zone II is the deformation zone and is surrounded by two cylindrical velocity discontinuity surfaces $S_1$ and $S_2$ as well as the punch surface. In addition to these surfaces, there are two frictional surfaces between material and container for plane strain extrusion type II as shown in Fig. 1b. The punch surface, which is labeled as $\psi(r)$ in Fig. 1, is given in the cylindrical coordinate system, $(r, \theta, z)$, where $\psi(r)$ is the angular position of the punch surface as a function of the radial distance from the origin. The origin of cylindrical coordinate system is located at point O which is defined by the intersection of the strip midline with a line that goes through the point where the punch begins and the exit point of the punch. The cylindrical velocity discontinuity surface $S_1$ is located at distance $r_o$ from the origin and the cylindrical velocity discontinuity surface $S_2$ is located at distance $r_f$ from the origin. The mathematical equations for radial positions of two velocity discontinuity surfaces $S_1$ and $S_2$ are given by

$$r_o = \frac{t_o}{\sin\alpha}, \qquad r_f = \frac{t_f}{\sin\alpha} \tag{2}$$

where $\alpha$ is the angle of the line connecting the initial point of the curved punch to the final point of the punch and

$$\tan\alpha = (t_o - t_f)/L \tag{3}$$

where $L$ denotes punch length.

### 2.1 Admissible velocity field

The first step in the upper bound analysis is to choose an admissible velocity field. The velocity field that has

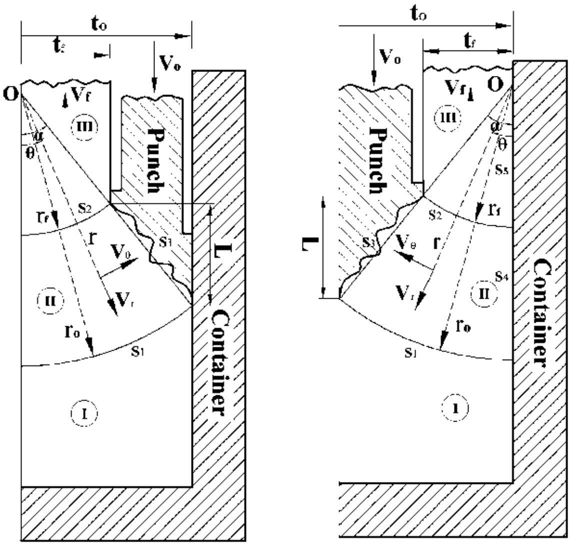


**Fig. 1** Schematic diagram of half-section of plane strain extrusion to show the derivation of the velocity field for: (**a**) type I and (**b**) type II

been derived from incompressibility condition and satisfies the velocity boundary conditions is a kinematically admissible velocity field. Volume constancy in cylindrical coordinate system is defined as

$$\dot{\varepsilon}_{rr} + \dot{\varepsilon}_{\theta\theta} + \dot{\varepsilon}_{zz} = 0 \tag{4}$$

where $\dot{\varepsilon}_{ii}$ is the normal strain rate component in the $i$-direction. The strain rates components in cylindrical coordinates are defined as

$$\begin{aligned}
\dot{\varepsilon}_{rr} &= \frac{\partial V_r}{\partial r} \\
\dot{\varepsilon}_{\theta\theta} &= \frac{1}{r}\frac{\partial V_\theta}{\partial \theta} + \frac{V_r}{r} \\
\dot{\varepsilon}_{zz} &= \frac{\partial V_z}{\partial z} \\
\dot{\varepsilon}_{r\theta} &= \frac{1}{2}\left(\frac{\partial V_\theta}{\partial r} + \frac{1}{r}\frac{\partial V_r}{\partial \theta} - \frac{V_\theta}{r}\right) \\
\dot{\varepsilon}_{\theta z} &= \frac{1}{2}\left(\frac{\partial V_\theta}{\partial z} + \frac{1}{r}\frac{\partial V_z}{\partial \theta}\right) \\
\dot{\varepsilon}_{zr} &= \frac{1}{2}\left(\frac{\partial V_r}{\partial z} + \frac{\partial V_z}{\partial r}\right)
\end{aligned} \tag{5}$$

Then, the velocity components for plane strain extrusion, types I and II shown in Figs. 1a–1b, can be given by

$$\begin{aligned}
V_r &= V_o\left(1 - \frac{r_o}{r}\frac{\sin\alpha}{\sin\psi}\right)\cos\theta \\
V_\theta &= -V_o\left(1 + r_o\frac{\sin\alpha}{\sin\psi}\frac{\partial\psi}{\partial r}\frac{1}{\tan\psi}\right)\sin\theta \\
V_z &= 0
\end{aligned} \tag{6}$$

The proposed velocity field satisfies volume constancy, Eq. (4), and the boundary conditions on surfaces $S_1$–$S_4$, therefore it is a kinematically admissible velocity field for deformation zone II.

Based on the established velocity field, the strain rate field for deformation zone can be obtained by Eq. (5) as

$$\begin{aligned}
\dot{\varepsilon}_{rr} &= -\dot{\varepsilon}_{\theta\theta} = V_o\frac{r_o}{r^2}\frac{\sin\alpha}{\sin\psi}\left(1 + r\frac{\partial\psi}{\partial r}\frac{1}{\tan\psi}\right)\cos\theta \\
\dot{\varepsilon}_{r\theta} &= \frac{V_o}{2}\left\{-\frac{1}{r} + r_o\frac{\sin\alpha}{\sin\psi}\frac{1}{\tan\psi}\left[\frac{1}{r^2}\tan\psi \right.\right. \\
&\quad + \left(\frac{\partial\psi}{\partial r}\right)^2\frac{1}{\tan^2\psi} - \frac{\partial^2\psi}{\partial r^2} \\
&\quad \left. + \left(\frac{\partial\psi}{\partial r}\right)^2\left(\frac{1+\tan^2\psi}{\tan\psi}\right)\right] \\
&\quad \left. + \frac{1}{r}\left(1 + r_o\frac{\sin\alpha}{\sin\psi}\frac{\partial\psi}{\partial r}\frac{1}{\tan\psi}\right)\right\}\sin\theta \\
\dot{\varepsilon}_{zz} &= \dot{\varepsilon}_{\theta z} = \dot{\varepsilon}_{zr} = 0
\end{aligned} \tag{7}$$

With the strain rate field and the velocity field, the standard upper bound method can be implemented. This upper bound model involves calculating the internal power of deformation over the deformation zone volume, calculating the shear power losses over the surfaces of velocity discontinuity, and the frictional power losses along frictional surfaces. Since, no deformation occurs in zones I and III, therefore, the strain rate components are zero.

### 2.2 Internal power of deformation

The internal power of deformation in an upper bound model is

$$\dot{W}_i = \frac{2}{\sqrt{3}}\sigma_0\int_v\sqrt{\frac{1}{2}\dot{\varepsilon}_{ij}\dot{\varepsilon}_{ij}}\,dv \tag{8}$$

Internal power of zones I, and III are zero and the equation to calculate the internal power of deformation in zone II is

$$\dot{W}_i = \frac{2\sigma_0}{\sqrt{3}}b\int_{r_f}^{r_o}\int_0^{\psi(r)}\sqrt{\frac{1}{2}\dot{\varepsilon}_{rr}^2 + \frac{1}{2}\dot{\varepsilon}_{\theta\theta}^2 + \dot{\varepsilon}_{r\theta}^2}\,r\,d\theta\,dr \tag{9}$$

where $b$ is width of the strip and $\sigma_0$ is the mean flow stress of the strip material and is given by

$$\sigma_0 = \frac{\int_0^{\varepsilon} \sigma \, d\varepsilon}{\varepsilon}, \qquad \varepsilon = \ln \frac{t_o}{t_f} \tag{10}$$

2.3 Shear power losses

The equation for the power losses along a shear surface of velocity discontinuity is

$$\dot{W}_S = \frac{\sigma_0}{\sqrt{3}} \int_{S_v} |\Delta V| \, dS \tag{11}$$

The shear power losses along the velocity discontinuity surfaces $S_1$ and $S_2$ can be given by

$$\dot{W}_{S_1} = \frac{\sigma_0}{\sqrt{3}} V_o r_o b \times \int_0^{\alpha} \left( 1 + \frac{r_o}{\tan\alpha} \frac{\partial \psi}{\partial r} \bigg|_{r=r_o} \right) \sin\theta \, d\theta \tag{12}$$

$$\dot{W}_{S_2} = \frac{\sigma_0}{\sqrt{3}} V_o r_f b \times \int_0^{\alpha} \left( 1 + \frac{r_o}{r_f} + \frac{r_o}{\tan\alpha} \frac{\partial \psi}{\partial r} \bigg|_{r=r_f} \right) \sin\theta \, d\theta \tag{13}$$

2.4 Friction power losses

The general equation for the friction power losses for a surface with a constant friction factor $m$ is

$$\dot{W}_f = m \frac{\sigma_0}{\sqrt{3}} \int_{S_f} |\Delta V| dS \tag{14}$$

For punch surface $S_3$

$$dS_3 = b \sqrt{1 + \left( r \frac{\partial \psi}{\partial r} \right)^2} dr \tag{15}$$

$$|\Delta V_3| = \big| (V_r - V_o \cos\psi) \cos\eta + (V_\theta + V_o \sin\psi) \sin\eta \big|_{\theta=\psi} \tag{16}$$

where $\eta$ is local angle of the punch surface with respect to the local radial velocity component and

$$\cos\eta = \frac{1}{\sqrt{1 + (r \frac{\partial \psi}{\partial r})^2}}, \qquad \sin\eta = \frac{r \frac{\partial \psi}{\partial r}}{\sqrt{1 + (r \frac{\partial \psi}{\partial r})^2}} \tag{17}$$

The frictional power losses along the punch surface is calculated as

$$\dot{W}_{f_3} = m \frac{\sigma_0}{\sqrt{3}} b \int_{r_f}^{r_o} |\Delta V_3| \sqrt{1 + \left( r \frac{\partial \psi}{\partial r} \right)^2} dr \tag{18}$$

Along the container surface, $S_4$, we have

$$|\Delta V_4| = |V_r|_{\theta=0}| = -V_o \left( 1 - \frac{r_o}{r} \frac{\sin\alpha}{\sin\psi} \right) \tag{19}$$

$$dS_4 = b \, dr \tag{20}$$

Replacing Eqs. (19) and (20) into Eq. (14) and integration, the frictional power along surface $S_4$ is given by

$$\dot{W}_{f_4} = m \frac{\sigma_0}{\sqrt{3}} V_0 b \int_{r_f}^{r_o} \left( \frac{r_o}{r} \frac{\sin\alpha}{\sin\psi} - 1 \right) dr \tag{21}$$

Along the container surface, $S_5$, we have

$$\dot{W}_{f_5} = m \frac{\sigma_0}{\sqrt{3}} V_f b r_f \cos\alpha \tag{22}$$

Based on the upper bound model, the required total power for a plane strain backward extrusion process obtained by summing the internal power and the power dissipated on all frictional and velocity discontinuity surfaces. Therefore, the total upper bound solution for extrusion force, for plane strain extrusion type I, is given by

$$F_I = \frac{\dot{W}_i + \dot{W}_{S_1} + \dot{W}_{S_2} + \dot{W}_{f_3}}{b V_0} \tag{23}$$

For plane strain extrusion type II, the extrusion force is determined by

$$F_{II} = \frac{\dot{W}_i + \dot{W}_{S_1} + \dot{W}_{S_2} + \dot{W}_{f_3} + \dot{W}_{f_4} + \dot{W}_{f_5}}{b V_0} \tag{24}$$

A MATLAB program has been implemented for the previously derived equations and is used to study the plane strain extrusion process for different punch shapes and different process conditions. It includes a parameter $L$, punch length, which should be optimized.

## 3 Comparison of FEM and analytical results

The developed velocity field and the upper bound model can be used for both types of plane strain extrusion, types I and II shown in Figs. 1a–1b, through punches of any possible shape if the punch profile is expressed as equation $\psi(r)$. To compare the upper bound results obtained for the types I and II with FEM simulation data, two types of punch shapes are examined in the present investigation. The first punch shape is a wedge shaped punch. This punch shape has a single constant value, i.e. $\psi(r)=\alpha$. The second punch shape is from the work by Yang and Han [9, 10]. They created a streamlined curved shape as a fourth-order polynomial whose slope is parallel to the axis at both entrance and exit. The equation describing the shape of Yang and Han curve is [21]

$$\begin{aligned}\frac{r}{r_o}\frac{\sin\psi}{\sin\alpha} &= 1+\left(\frac{C_f}{(1-t_f/t_o)^2}-\frac{3}{1-t_f/t_o}\right)\\ &\quad\times\left(-\frac{r}{r_o}\frac{\cos\psi}{\cos\alpha}+1\right)^2\\ &\quad+\left(\frac{2}{(1-t_f/t_o)^2}-\frac{2C_f}{(1-t_f/t_o)^3}\right)\\ &\quad\times\left(-\frac{r}{r_o}\frac{\cos\psi}{\cos\alpha}+1\right)^3\\ &\quad+\frac{C_f}{(1-t_f/t_o)^4}\left(-\frac{r}{r_o}\frac{\cos\psi}{\cos\alpha}+1\right)^4 \qquad (25)\end{aligned}$$

where

$$C_f=\frac{3(1-t_f/t_o)(1-2L_f/L)}{1-6L_f/L+6(L_f/L)^2} \qquad (26)$$

where $L_f/L$ represents the position of the inflection point for the sigmoid profile and can vary from 0 to 1 and $L$ denotes punch length.

The initial strip was lead with the flow stress given by tensile test as

$$\sigma=38.97\varepsilon^{0.436}\ \text{(MPa)} \qquad (27)$$

The mean flow stress of the lead material is given by Eq. (10) and is used in the analysis.

The extrusion force for plane strain backward extrusion through a wedge shaped punch and the Yang and Han punch shape obtained from the upper bound model, for $t_o/t_f=2$, $t_o=10$ mm and $m=0.2$, are compared with each other in Figs. 2a–2b. As it is shown, the extrusion force of Yang and Han punch shape is lower the wedge shaped punch.

The plane strain extrusion processes have been simulated using the finite element software, ABAQUS. Due to the symmetry of the process, the finite element meshes are generated on the half cross-section of the strip. The type of the element used in the model is a quadratic structured plane strain element, CAX4R

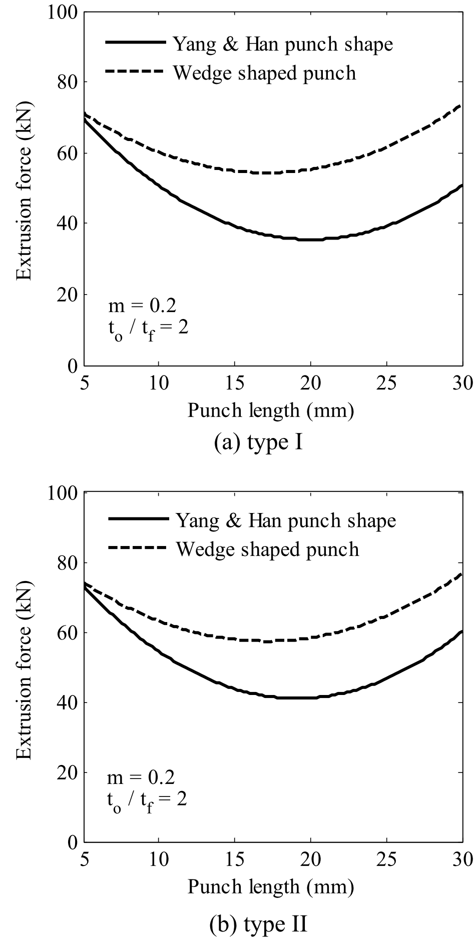


**Fig. 2** Comparison between upper bound results for Yang and Han die shape and the wedge shaped die for $t_o/t_f=2$ and $m=0.2$

element. Figure 3a illustrates the mesh used to analyze the deformation and Fig. 3c shows the geometry of the deformed mesh for type I. Figure 3b illustrates the mesh used to analyze the deformation and Fig. 3d shows the geometry of the deformed mesh for type II. Punch and container undergo elastic strains only. Thus, it is not necessary to use a fine mesh in these two pieces. However, sufficiently fine meshing is essential in strip material which undergoes plastic deformation. The container is fixed by applying displacement constraint on its nodes while the punch model is loaded by specifying displacement in the $\theta=0$, direction. Deformed models are shown in Figs. 3b and 3c, respectively.

Two punches are used in the simulations: (a) the optimum wedge shaped punch and (b) the optimum

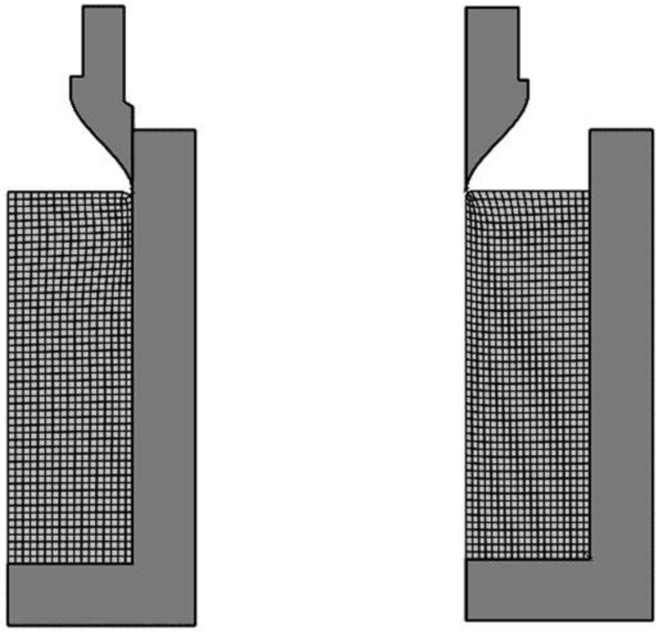

(a) The finite element mesh of type I (b) The finite element mesh of type II

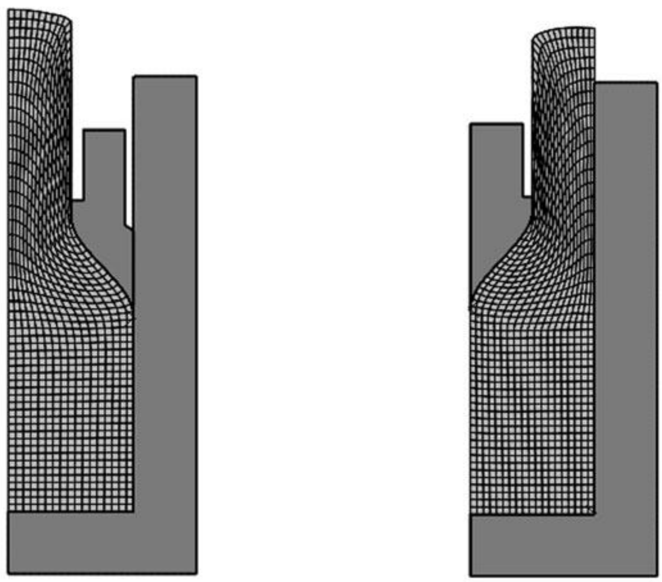

(c) The deformed mesh of type I (d) The deformed mesh of type II

**Fig. 3** The finite element mesh and the deformed mesh for plane extrusion backward extrusion

Yang and Han punch shape. In Figs. 4a–4b, the extrusion force of two punches obtained from the upper bound solution and the FEM simulation is compared with each other. The results show a good agreement between the analysis and FEM. As shown in Fig. 4, the theoretically predicted force is higher than the FEM results, which is due to the nature of the upper bound theory. The results also demonstrate that extrusion force of an optimum streamlined punch is less than the optimum wedge shaped punch. As shown

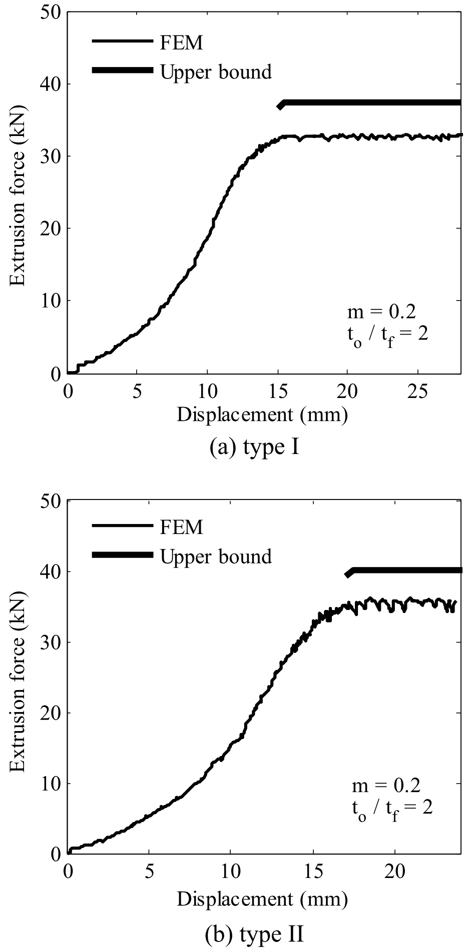


**Fig. 4** Comparison of analytical and FEM force-displacement curves for Yang and Han punch shape: (**a**) type I and (**b**) type II

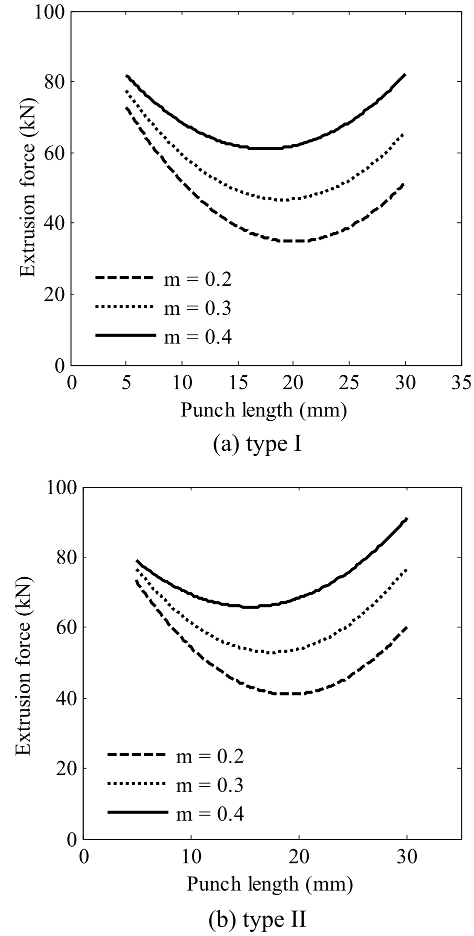


**Fig. 5** Effect of friction factor upon the extrusion force for Yang and Han punch shape for: (**a**) type I and (**b**) type II

in this figure, at the early stage of extrusion, unsteady state deformation occurs, and the materials have not yet filled up the cavity of the punch completely. Thus, the extrusion force increases as the extrusion process proceeds. After the materials have filled up the cavity of the punch completely, the extrusion force is constant.

The effect of friction factor upon extrusion force for two types of plane strain extrusion process is shown in Figs. 5a and 5b. As shown in these figures, at a punch length that is called the optimum length, the extrusion force is minimized. As shown in this figure, the extrusion force increases with increasing the friction factor. Also, with increasing the friction factor, the optimum length of punch is decreased.

## 4 Conclusions

In this paper a generalized velocity field and power terms for plane strain backward extrusion through punches of any shape were presented and the following results are extracted:

1. The theoretical predicted extrusion forces are in good agreement with the FE results.
2. The developed upper bound solution can be used for fast estimation of extrusion force in plane strain backward extrusion and for a given process conditions, it can be used for finding the optimum punch length which minimizes the extrusion force.
3. The optimum length of punch decreases with increasing the friction factor.

## References


1. Avitzur B (1963) Analysis of wire drawing and extrusion through conical dies of small cone angle. ASME J Eng Ind 85:89–96
2. Avitzur B (1964) Analysis of wire drawing and extrusion through conical dies of large cone angle. ASME J Eng Ind 86:305–316
3. Avitzur B (1966) Flow characteristics through conical converging dies. ASME J Eng Ind 88:410–420
4. Avitzur B (1967) Strain-hardening and strain-rate effects in plastic flow through conical converging dies. ASME J Eng Ind 89:556–562
5. Hillier MJ, Johnson W (1963) Plane strain extrusion through partially rough curved dies. Int J Mech Sci 5:191–201
6. Avitzur B (1968) Metal forming: processes and analysis. McGraw-Hill, New York
7. D'Alia FS (1969) Drawing and extruding: theoretical and approximate formulas. Meccanica 4(1):67–77
8. Chen CT, Ling FF (1968) Upper bound solutions to axisymmetric extrusion problems. Int J Mech Sci 10:863–879
9. Zimmerman Z, Avitzur B (1970) Metal flow through conical converging dies—a lower upper bound approach using generalized boundaries of the plastic zone. ASME J Eng Ind 92:119–129
10. Yang DY, Han CH, Lee BC (1985) The use of generalized deformation boundaries for the analysis of axisymmetric extrusion through curved dies. Int J Mech Sci 27:653–663
11. Yang DY, Han CH (1987) A new formulation of generalized velocity field for axisymmetric forward extrusion through arbitrarily curved dies. ASME J Eng Ind 109:161–168
12. Chen CT, Ling FF (1968) Upper-bound solutions to axisymmetric extrusion problems. Int J Mech Sci 10:863–879
13. Nagpal V (1974) General kinematically admissible velocity fields for some axisymmetric metal forming problems. ASME J Eng Ind 96:1197–1201
14. Chen CC, Oh SI, Kobayashi S (1979) Ductile fracture in axisymmetric extrusion and drawing—Part 1: Deformation mechanics of extrusion and drawing metal. ASME J Eng Ind 101:23–35
15. Liu TS, Chung NL (1990) Extrusion analysis and workability prediction using finite element method. Comput Struct 36:369–377
16. Kim NH, Kang CG, Kim BM (2001) Die design optimization for axisymmetric hot extrusion of metal matrix composites. Int J Mech Sci 43:1507–1520
17. Weinberger HF (2003) Necessary conditions for the optimality of an extrusion die for a rigid-plastic material. Meccanica 38:547–554
18. Bakhshi-Jooybari M, Saboori M, Hosseinipour SJ et al (2006) Experimental and numerical study of optimum die profile in backward rod extrusion. J Mater Process Technol 177:596–599
19. Saboori M, Bakhshi-Jooybari M, Noorani-Azad M et al (2006) Experimental and numerical study of energy consumption in forward and backward rod extrusion. J Mater Process Technol 177:612–616
20. Gordon WA, Van Tyne CJ, Moon YH (2007) Axisymmetric extrusion through adaptable dies. Part 1. Flexible velocity fields and power terms. Int J Mech Sci 49:86–95
21. Gordon WA, Van Tyne CJ, Moon YH (2007) Axisymmetric extrusion through adaptable dies. Part 2. Comparison of velocity fields. Int J Mech Sci 49:96–103
22. Gordon WA, Van Tyne CJ, Moon YH (2007) Axisymmetric extrusion through adaptable dies—Part 3: Minimum pressure streamlined die shapes. Int J Mech Sci 49:104–115
23. Haghighat H, Amjadian P (2011) A generalized velocity field for plane strain extrusion through arbitrarily curved dies. J Manuf Sci E-T ASME 133:041006